Effect of charge transfer on band alignment in 2D|3D heterostructures: A study of $HfS_2|HfO_2$ interfaces

Ned Thaddeus Taylor [*] and Steven Paul Hepplestone [†]
Department of Physics, University of Exeter, Stocker Road, Exeter, EX4 4QL, United Kingdom

(Received 6 January 2023; revised 30 March 2023; accepted 12 April 2023; published 9 May 2023)

$HfS_2|HfO_2$ interfaces present a uniquely interesting study in band alignment. The band alignment between materials determines the viability of many electronic devices. We have modeled a variety of two-dimensional|three-dimensional (2D|3D) interfaces $HfS_2|HfO_2$ interfaces, showing that the band alignment can change substantially depending on the geometric alignment. Our results have shown that there exists almost no electronic reconstruction when layers of HfS_2 are placed on a HfO_2 substrate. Conversely, when the in-plane connection between HfS_2 and HfO_2 is made (lateral), there is a more significant interface reconstruction present. In the latter case, all examples considered yielded a type I alignment, whereas in the case that layers were parallel to the HfO_2 substrate (stacked) we found that the alignment was either type I or type II with a very small difference between the valance band offsets of the two constituents. We show that the range in the barrier heights between these two systems can vary by up to 2.46 eV. This variation is driven by the amount of charge transfer across the interface and indicate that 2D|3D interfaces have considerably more tunability in their band alignment than 2D|2D or 3D|3D interfaces.

DOI: 10.1103/PhysRevB.107.205302

I. INTRODUCTION

The increased density of electronic components on chips has resulted in increased need for high-*k* dielectrics. Forming such a high-*k* dielectric ideally needs to be performed *in situ*. Recently, laser oxidation has been applied to HfS_2 to form $HfS_2|HfO_2$ devices [1–4], providing a route to direct *in situ* fabrication. Due to its high chemical and thermal stability, high band gap, and high dielectric constant [5–7], HfO_2 has been considered as a replacement of SiO_2 as a gate dielectrics for electron and hole barriers. As a high-*k* dielectric, HfO_2 is used in capacitors for microelectronics [8–10]; and as a gate dielectric in emerging two-dimensional electronics [11–13]. In addition, HfO_2 is considered a leading candidate for memristor applications [14–16] and its implementation at the nanoscale would allow these devices to flourish.

The chemical instability of HfS_2 in air (due to oxidation) is used to promote easy oxidation into HfO_2. This is either done through simple means of heating (such as annealing), or through laser oxidation. The growth width of HfS_2 flakes using chemical vapor deposition has increased in recent years to the scale of tens of microns [17,18]. Larger-area methods have been presented using inkjet processes [4]. Larger flake widths will allow for larger $HfS_2|HfO_2$ devices and more devices to be fabricated on single samples. HfO_2 has also been explored as a means of improving HfS_2 properties (such as mechanical, dielectric, and electronic) for applications in stretchable electronics and transistors [19–21]. With a growing interest, understanding the interactions between these two materials and the subsequent interfaces is key to determining how these will work as devices.

With the ease of forming $HfS_2|HfO_2$ interfaces via laser oxidising channels of HfS_2 into HfO_2 [2], the question starts to arise whether the HfO_2 formed is two-dimensional (2D) layered, taking on the crystal structure of HfS_2 transition metal dichalcogenide (TMDC), or whether it has formed a three-dimensional (3D) crystal, typical of HfO_2. If the HfO_2 is 3D, then the interface will be unlike others explored before, due to the way in which the 2D and 3D materials could align. While some work has shown 3D-like crystal structures of HfO_2 at the interface [22] (using STEM), others point towards 2D-like phase of HfO_2 due to the large basal spacing of HfS_2 remaining in HfO_2 after oxidation [3]. It is therefore possible that the phase of HfO_2 is strongly dependent on the growth process, with thermal annealing leading to 3D HfO_2, while laser oxidation may form 2D HfO_2. The consequences for the electronic properties of both these phases of HfO_2 should be considered.

Interfaces between 2D-TMDC structures has been explored extensively in recent history, with studies exploring both lateral and stacked 2D|2D heterostructures [23–25]. Interest is often focused on the band gap of the subsequent structure. Interfaces between 2D and 3D interfaces have also been observed and explored in many systems. Many such systems involve the 2D layered material being deposited or layered on top of a 3D substrate (i.e., a stacked interface), which has seen a lot of attention over the years [26–30].

[*] n.t.taylor@exeter.ac.uk
[†] s.p.hepplestone@exeter.ac.uk

Published by the American Physical Society under the terms of the Creative Commons Attribution 4.0 International license. Further distribution of this work must maintain attribution to the author(s) and the published article's title, journal citation, and DOI.

However, another configuration of joining 2D – or one-dimensional (1D) – materials and 3D materials exists, where the 2D material is joined end-on to the 3D material; this can be seen in some contacts, molecules linking 3D materials, in addition to the growth of nanoforests, and vertical nanosheets [26,31,32]. These end-on interfaces are described here as lateral interfaces due to their geometric similarity with 2D|2D lateral interfaces. Understanding how the lateral vs stacked interfaces changes the electronic properties is vital to understanding how growth is affecting devices.

A chief characteristic of interfaces is the band alignment. While there exist simple methods to predict band alignment of semiconductor-semiconductor heterojunctions (Anderson's rule [33]) and metal-semiconductor heterojunctions (Schottky-Mott model [34–36]), these have been proven to be inaccurate for most real systems. Further approaches in terms of interface states, metal-induced gap states and charge neutrality level can rectify some of these shortcomings and provide direct analytical insight, but due to the scale of the interfaces where local reconstruction can have affects on the form of the local field first principles approaches have become necessary. As density-functional theory (DFT) has become more widespread, it has been applied to band-alignment problems [37–40]. The use of DFT showed that metal-induced gap states (induced density of interface states) tend to form at metal-semiconductor interfaces (semiconductor heterojunctions), and that these decay exponentially into the semiconductor. While it can be used to compare the hole affinities of materials, a more accurate method that accounts for subsequent interactions involves modeling interfaces. This computational method has shown great accuracy [41,42]. Recently, more methods have tried to combine the simplicity of analytical methods and the accuracy of the DFT method without the need to model complex interface systems [43]. Similarly, Anderson's rule has gained renewed interest in recent years due to its simplicity and the strong predictive nature it offers for two-dimensional van der Waals (vdW) heterostructures [44]—although this has also been proven to break in some cases [45]. The effectiveness of these rules for 2D|3D heterojunctions has not been thoroughly explored as of yet.

In this article, we study, using a first principles approach based on DFT, the role of surface orientation and termination on the interface between HfS_2 (a nominally 2D material) with HfO_2, a bulk material in the monoclinic phase, with a particular focus on band alignment. We consider the two extrema of interfaces between 2D and 3D systems. These can either be parallel surface normal interfaces (which we henceforth call *stacked*) or perpendicular surface normal interfaces (which we will call *lateral*), as detailed in Fig. S1 of the Supplemental Material [46]. Between these two extrema, there can be a continuous range of angles made between the 2D and 3D systems. The most commonly considered type of interface between 2D and 3D systems is the stacked form. Here, we explore both stacked and the less well explored lateral interfaces between 2D and 3D materials. We discuss the effect these different interfaces have on the band alignment, charge transfer, and further electronic properties as well as their consequences for excitonic setups.

II. COMPUTATIONAL METHODS

In this work, we have employed first principles DFT techniques to explore the structural, electronic, and optical properties of $HfS_2|HfO_2$ interface systems, and the constituents. The VASP [47,48] software package was used to perform the calculations. The valence electrons for each atomic species are considered as follows: Hf $6s^2 5d^2$, S $3s^2 3p^4$, O $2s^2 2p^4$. The projector augmented wave method was used to describe the interaction between core and valence electrons, and a plane-wave basis set was used with an energy cutoff of 700 eV. All calculations were completed using the Perdew-Burke-Ernzerhof (PBE) [49] functional. PBE was chosen due to the scale of the structures and small error it creates in band alignment of occupied states [41]. All forces are relaxed to less than 0.01 eV/Å per atom, and electronic self-consistency is accurate to within 10^{-7} eV. Structural relaxations are performed at a k-point spacing of at most 0.04 Å^{-1} along each reciprocal-lattice vector, while electronic calculations (such as density of states) were performed using a maximum k-point spacing of 0.02 Å^{-1}. Density of states plots are presented with a smearing sigma equivalent to 0.03 eV.

While various phases were considered and explored for HfO_2, the phase presented in this work is predominantly the monoclinic phase with space group $P2_1/c$. The T-phase was used for bulk HfS_2, space group $P\bar{3}m1$. Initial bulk perfect crystals for HfS_2 and HfO_2 were obtained from the Materials Project database [50,51], with subsequent structural relaxations then performed usingVASP. The relaxed lattice constants of bulk T-phase HfS_2 used are $a = 3.644$ Å, and $a/c = 0.533$. Non-vdW spacing was used for lattice matching, but the inclusion of vdW correction was not found to change the results. The a value is overestimated from experiment by around 0.6%, but the c axis is an overestimation of around 16% [52]. HfO_2 lattice constants after relaxation were as follows: $a = 5.139$ Å, $b = 5.188$ Å, $c = 5.315$ Å, $\beta = 99.81^\circ$. The HfO_2 lattice constants agree with experimental results to within 0.4% [53]. HfS_2 was found to have an indirect band gap of 1.239 eV between Γ and M. HfO_2 was found to have an indirect gap of 3.952 eV between Γ and X. All values presented here are obtained using the PBE GGA functional, which is known to underestimate band gaps. The experimental gaps of HfS_2 and HfO_2 in the above phases are 2.85 and 5.65 eV, respectively [54]. It should be noted that the key focus of this work is not on the experimental accuracy of the band gaps and band offsets. This work is meant to be a qualitative study highlighting how, within the same consistent approach, there exists a difference in band alignment between lateral and stacked interfaces (see Supplemental Material Sec. SIII for further discussion [46]).

All slab and interface structures are generated using the ARTEMIS software package [55]. The largest vector and angular mismatch of the interfaces discussed here are 4.07% and 0.004°, respectively [both correspond to the $(010)/(1\bar{1}1)$ interface]. Further details regarding the structural setup of the interfaces can be found in Table SI of the Supplemental Material [46]) All interfaces generated use stoichiometric slabs, where the HfS_2 regions are terminated on sulfur atoms, and the HfO_2 regions are terminated on oxygen. Slab calculations were performed using a 14 Å vacuum gap to minimize

spurious interactions between surfaces. All of the HfS_2 and HfO_2 slabs are nonpolar and are mirrored around the center of the slab, meaning that their two surfaces are symmetrically equivalent. With this, the interfaces formed from the two slabs should also be symmetrically equivalent; in doing so, we are, in effect, modeling two mirror images of the same interface in our simulation, preventing the appearance of any spurious electric fields across the system. For further discussions on the choice of surface plane, termination, and stoichiometry, see Secs. SIII and SXII of the Supplemental Material [46]). All comparisons are between the slab and interface structures are done using the isolated strained slabs; this choice is made to decouple and account for any energetic or electronic effects introduced by strains (see Sec. SVI for further discussions [46], in addition to comparison to unstrained slabs).

In each layer-projected density of states (LDOS) presented in this work, the layers here are defined as the shortest region along c that contains a complete number of primitive formula units. The states associated with all atoms in a single layer are summed to form a layer-projected density of states; this is performed for every layer in the system, then the new densities of states are plotted next to each other to allow for comparison between layers.

Band alignment is identified using the method as outlined by Delaney *et al.* [56]. The macroscopic average is obtained by taking the running average over the local potential, where the running average is performed on a subset of data that has a width equal to the dominant periodic feature (parallel to the direction averaging over) within the system. For the case of an interface system, there exist multiple periodic features (i.e., the layer spacing of the two constituent materials); in such a system, the running average is performed multiple times over these multiple dominant periodic features until the macroscopic average is sufficiently smooth within the two separate regions (i.e., the two materials), but with both regions still distinct from each other.

Charge-transfer plots are generated by taking the charge density of the interface and deducting the charge densities of the individual slabs that are present in the system. For this situation only, the slabs are generated by removing the adjoining slab of the other material from the relaxed interface structure; no atomic relaxations are performed on these slabs. The resultant charge densities of these unrelaxed slabs are deducted from the relaxed interface to provide the charge-transfer density associated with trans-interfacial bonds. Finally, the charge-transfer density within planes parallel to the interface are summed and normalized with respect to the area of the interface. This gives us a 1D charge-transfer plot running perpendicular to the interface.

The energy of forming an interface between two materials (formation energy) is defined as the energy difference between the interface system and the constituent crystals in their lowest energy bulk phases, divided by two times the area of the interface (due to the two equivalent interfaces modeled within the cell),

$$E_{\text{form,b}} = \frac{E_{\text{interface}} - (nE_{\text{bulk,HfS}_2} + mE_{\text{bulk,HfS}_2})}{2S}, \quad (1)$$

where n and m are number of units of HfS_2 and HfO_2 in the interface system, respectively. $E_{\text{interface}}$ is the energy of the interface structure, and $E_{\text{bulk,A}}$ is the energy of material A in the bulk. S is the area of the interface plane within one periodic cell. The division by the area allows for a direct comparison of energies, regardless of the size of the cell parallel to the interface. A lower formation energy relates to a more energetically favorable interface than that of one with a higher formation energy. If a formation energy is negative, then it is energetically more favorable to form than the two constituent bulks. Another method can be used to define formation energy, which involves comparing the energy of the interface structure to the constituent slabs,

$$E_{\text{form,s}} = \frac{E_{\text{interface}} - (E\,\text{slab, HfS}_2 + E_{\text{slab,HfO}_2})}{2S}. \quad (2)$$

Here, $E_{\text{slab,A}}$ is the energy associated with a slab of material A. This ignores the energy cost of cleaving the two slabs and, instead, focuses on the energy required to bring two slabs together and form trans-interfacial bonds. When using this formation energy, we give it with respect to the slabs with the same surface terminations as are found in the respective interface structure.

III. RESULTS

A. Geometric and energetic properties

The $HfS_2|HfO_2$ interface can exhibit many different geometries depending on how the constituent materials are grown. In Fig. 1, we present the six different geometries considered in this work. These geometries provide a selective sample covering both 2D|3D and 2D|2D interfaces, both lateral and stacked alignment, and exhibiting differing strains. A comparison between interfaces B and E (C and F) provides a direct comparison of the lateral and stacked interfaces [with both B and E involving (110)-terminated HfO_2, and C and F involving $(\bar{1}11)$-terminated HfO_2], with only the joining angle of the HfS_2 to the HfO_2 differing between them. To make this comparison, we have strained the HfO_2 by up to 4.1%, which lies within the tolerances typically observed in interfaces in experiment [57–60].

An initial study of the six interfaces reveals that lateral interfaces result in some tilting, bending, or twisting of the HfS_2 layers, whereas the stacked do not. We define the three types of large distortion: tilt, bend, and twist in the Supplemental Material (see Fig. S2 [46]). Conversely, in both lateral and stacked interfaces, the HfO_2 shows no substantial change in structure from its periodic monoclinic bulk structure. In the stacked interfaces, very little reconstruction occurs for either material. Comparison of these finds that the lateral interfaces form Hf–S (Hf–O) covalent bonds of approximately 2.58 Å (2.12 Å), whereas the stacked form vdW-type bonding, with bond lengths of approximately 4.68 Å (5.31 Å). For the stacked systems, the average interlayer vacuum gap is 3.58 Å. The average bulk covalent Hf–S (Hf–O) bond length is 2.55 Å (2.15 Å), while the average bulk van der Waals Hf–S bond length is 5.79 Å, with an interlayer vacuum gap of 3.95 Å. These values demonstrate the low amount of distortion of the two constituents in the interface structures.

For the (010)-terminated HfS_2 (interfaces B and C), the HfS_2 surface is composed of Hf and S atoms, maintaining the 1 : 2 ratio (with all planes being composed of Hf and S

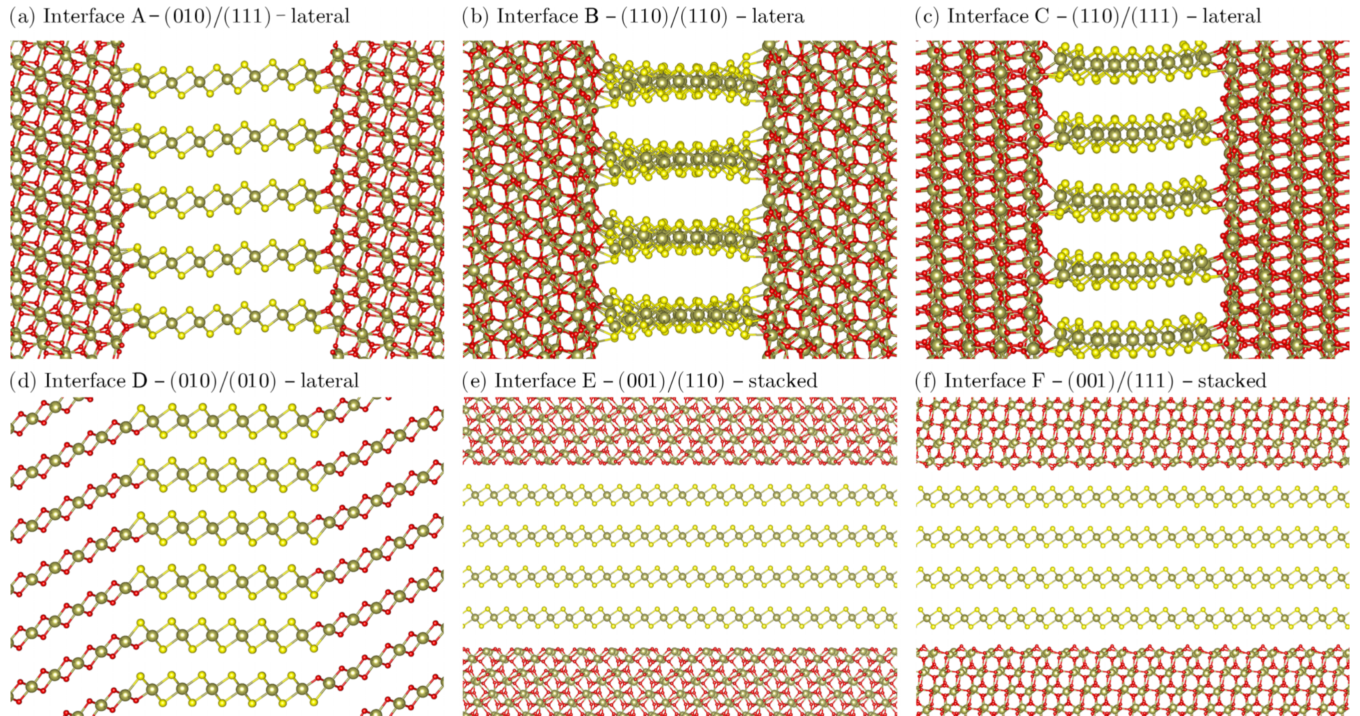

FIG. 1. Ball and stick models showing atomic structures of $HfS_2|HfO_2$ interfaces. The (a) $(010)/(1\bar{1}1)$, (b) (110)/(110), (c) $(110)/(\bar{1}11)$, (d) (010)/(010)–2D, (e) (001)/(110), and (f) $(001)/(\bar{1}11)$ heterostructures. In each subfigure, multiple unit cells are shown, and Hf, S, and O are represented as gold, yellow, and red, respectively.

atoms at the 1 : 2 ratio). For the other heterostructures, the HfS_2 surface atom is S, with the subsurface composed of Hf (then alternating between two planes of S atoms and one plane of Hf atoms).

The lateral interfaces are $HfS_2(010)/HfO_2(1\bar{1}1)$ (referred to as interface A), $HfS_2(110)/HfO_2(110)$ (interface B), and $HfS_2(110)/HfO_2(\bar{1}11)$ (interface C). They all exhibit similar geometric features—slight bending and/or tilting of the HfS_2, minor reconstruction of HfO_2 isolated to the surface level. For theses heterostructures, the tilting, bending, or twisting is caused by the two equivalent competing interfaces present within the periodic cell attempting to form the same interface bonding. This need for the HfS_2 to relax to a tilted form is due to the HfO_2 being monoclinic and, as such, its subsequent layers are offset from each other. In interface A, a slight tilting is exhibited by the HfS_2, as seen in Fig. 1(a). Note, however, that the tilt across the system is minor, around $4.0 \pm 1.5^\circ$ off of the 90° expected. In interface B, there is both twisting and bending of the HfS_2 layers [see Fig. 1(b)]. For interface C, we see slight bending of the HfS_2 layers, along with slight distortion of Hf and S bonds near the interface [see Fig. 1(c)]—this system exhibits the most significant reconstruction of HfS_2 out of the six heterostructures discussed here. With all of the lateral heterostructures, the HfO_2 region sees little atomic reconstruction overall, with minor changes near the surface (most significant in interface B). Overall, the small strains and tilting observed in the lateral structures are a direct result of the supercell choice, rather than a fundamental feature of the interface and the variety of scenarios considered provides insight into the general case of lateral $HfS_2|HfO_2$ interfaces.

The $HfS_2(010)/HfO_2(010)$ interface (interface D) is a special case. While it is a lateral interface, it is composed of both 2D HfS_2 and HfO_2 in a 2D TMDC-like T phase [this 2D phase is referred to by using the notation (010)/(010)–2D]. In this heterostructure, we see a tilting of the 2D HfO_2 with respect to the HfS_2 [see Fig. 1(d)]—this relates to a tilt angle of 27.5°. The HfS_2 and HfO_2 relax to meet each other at an angle at the interface, which is likely caused by the competing bonding-environment of either bulk. We explore bonds of interface D and identify an anisotropic strain applied to both the HfS_2 and HfO_2. We find that Hf–S (Hf–O) bonds parallel (perpendicular) to the interface plane are compressed for HfS_2 (HfO_2) by up to 2% when compared with bonds which are perpendicular (parallel), which remain close to their bulk counterparts (compressed bond-lengths of 2.50 Å for the Hf–S). It is also noted that the isolated (010)–2D slab of HfO_2 retained this anisotropic bonding after relaxing, whereas its bulk counterpart did not. The strain applied to the HfS_2 in this system can be likened to a shear strain applied along layered material plane—with this shear strain causing a reduction in the HfS_2 band gap.

In all four lateral heterostructures, we see tilting of the 2D layers. This is most likely due to the systems compensating for the different bonding angles of S–Hf–S and O–Hf–O. For the 2D|3D interfaces, it is likely that this is also caused by the symmetrically equivalent HfO_2 surfaces being offset (unaligned) from each other at both interfaces, thus requiring HfS_2 to tilt in order to bond to the same sites on the two equivalent surfaces. For the 2D|2D interface, this offset of surfaces is not present, meaning it is much more likely tilted due to the bond angle mismatch.

The stacked interfaces are $HfS_2(001)/HfO_2(110)$ (interface E) and $HfS_2(001)/HfO_2(\bar{1}11)$ (interface F). These structures demonstrate the typical 2D layer *resting* on a 3D bulk type

TABLE I. Energetics and electronic properties of different $HfS_2|HfO_2$ interfaces. The thickness and orientation of each of the two constituent materials is provided. The formation energies calculated with respect to the bulk crystals [Eq. (1)] and with respect to the strained constituent slabs [Eq. (2)]. The band offsets between the valence bands of the two constituents are presented, calculated with Anderson's rule and using the first principles approach outlined within the text. Lastly, the fundamental electronic gap is given. Lateral (stacked) type describes a system where the interface normal vector is perpendicular (parallel) to the vector normal to the plane of the HfS_2 layers. †HfO_2 is in a 2D phase in this interface system only (with energies and band offsets given with respect to this 2D-phase of HfO_2).

		HfS_2		HfO_2		E_{form} (eV/Å^2)		Band offset (eV)		
Name	Type	Plane	No. of layers	Plane	No. of layers	From bulk	From slabs	Anderson's rule	First principles	E_g (eV)
A	Lateral	(010)	7	$(1\bar{1}1)$	9	0.072	−0.064	0.32	1.90	1.34
B	Lateral	(110)	9	(110)	6	0.099	−0.044	−0.07	1.64	1.45
C	Lateral	(110)	9	$(\bar{1}11)$	6	0.088	−0.033	0.76	1.56	1.31
D	Lateral	(010)	6	(010)†	6	0.164	−0.126	0.70	1.80	0.43
E	Stacked	(001)	4	(110)	6	0.088	−0.002	−0.56	−0.56	0.69
F	Stacked	(001)	4	$(\bar{1}11)$	6	0.105	−0.001	0.24	0.26	1.24

geometry. Both these exhibit minimal reconstruction for both the HfS_2 and HfO_2. This is likely attributed to the large interlayer separation that dominates the interface instead of the shorter covalent bonding that is exhibited in the lateral interface. The HfS_2 region does not show any rippling effects associated with mismatching large 2D sheets to 3D bulk—this is due to the HfO_2 region being under strain and the HfS_2 regions having less than 0.1% strain. These structures are more akin to stacked 2D TMDC heterostructures [45] and are more typical of the interfaces explored in 2D|3D systems.

Interfaces B and E both contain the equivalent HfO_2 (110) surface, while allowing for direct comparison of a lateral and stacked interface. The two bulks have shown minimal disruption (as discussed earlier). Similarly, interfaces C and F show a comparison of the equivalent HfO_2 $(\bar{1}11)$ surface, allowing for direct comparison of a lateral and stacked interface. In both comparisons, we see that the HfS_2 in lateral systems has undergone a small amount of tilting in the layer, but the HfO_2 has undergone little change, allowing for a comparison of lateral and stacked interfaces.

Energy of formation helps provide insight into how likely the interfaces modeled are to occur, in addition to their relative abundances. By comparing our interface structures to their respective bulks [see Eq. (1)], we calculate the formation energies $E_{form,b}$ of the lateral interfaces, interfaces A, B, C, and D, as 0.072, 0.099, 0.088, and 0.164 eV/ Å^2 , respectively, and the stacked systems, interfaces E and F, as 0.088 and 0.105 eV/ Å^2 , respectively (see Table I). These results show that interface A exhibits the lowest formation energy out of all the considered interfaces. For the lateral interfaces, this is likely due to interface A involving the least reconstruction of all the lateral interfaces (in both the HfS_2 and HfO_2 regions) while still providing bond compensation for the broken surface bonds of the two constituents. We note that all interfaces (with the exception of interface D) exhibit comparable formation energies to A, and can thus still be considered as physical. This indicates that both lateral and stacked interfaces are highly feasible and depend on the growth process.

Interface E exhibits the lowest formation energy for the stacked interfaces, but not as low as A. When forming the surface of the HfO_2 in either system, dangling bonds are created, but in the lateral case these are compensated due to the direct bonding with HfS_2 that occurs at the interface, which does not occur in stacked interfaces. This results in the higher formation energy of stacked systems. However, the stacked interfaces do not show significantly higher formation energies than the lateral interfaces, and this is likely due to the energy required to cleave the covalent bonds of the HfS_2 in the first place. In the stacked interfaces, only van der Waals bonds are cleaved for the HfS_2, which is known to require a lot less energy.

The formation energies presented in Table I are comparable with those for 3D|3D interfaces [61], but are around four times higher than those seen in TMDC van der Waals heterostructure binding energies (typically 0.02 eV/Å^2) [62,63]. The increased energy cost is a result of three key points that need to be addressed regarding this comparison; first, the lateral interface is not a van der Waals heterostructure because it involves in-plane covalent bonding, which will significantly increase the energy of formation due to higher energies associated with covalent bonding over van der Waals bonding. Second, the stacked interface is a van der Waals bonding between a monolayer and a 3D crystal, which could lead to additional energy associated with other interactions. Finally, the energies presented here are formation energies in reference to the constituent bulks, meaning that the formation energy also includes the energy to cleave the two crystals and bind them together. To account for some of these concerns, we can also compare the values of $E_{form,s}$ [see Eq. (2)] for energy of cleaving, phase changes, and strain.

Using the slab relative formation energy ($E_{form,s}$), we obtain formation energies of −0.063, −0.022, and −0.072 eV/ Å^2 for interfaces A, B, and C, respectively. The two stacked systems, interfaces E and F, both have formation energies of −0.001 eV/ Å^2 (see Table I). These values for formation energy are much lower than when calculating from bulk, which is expected as cleavage and phase-change energies are mitigated here. The negative formation energies are highly indicative that the compensation of the bonds at the surface of these slabs is highly preferable.

Using the formation energy relative to slabs, we identify interface C as the most energetically favorable interface (with A still being close enough in energy to be physical). The change in most energetically favorable is likely due to two

factors: (i) the (110) termination cleaves more Hf–S bonds per Hf atom than the (010) termination, so formulating the formation energy relative to the slabs accounts for this higher cleavage energy (see Table SII [46]), and (ii) there is more bond compensation present in interface C than A. There is clearly a lot of energy gained when forming bonds at the interface from prior dangling bonds. This matches well with the stacked formation energies, as very little energy gain or loss occurs when forming these interfaces due to their trans-interfacial bonding being dominated by van der Waals bonds (which are comparatively low in energy).

For the special case of interface D, we see a very high formation energy when comparing with bulks, and a very low formation energy when comparing with the constituent slabs. The formation energy ($E_{\text{form,b}}$) is somewhat misleading here as it includes the energy difference between the 3D monoclinic phase and 2D T phase of HfO_2. Once you account for this energetic difference, the interface formation is very favorable. In addition, care must be taken when considering the formation energies ($E_{\text{form,b}}$ and $E_{\text{form,s}}$) as defining an area of interface for a lateral interface between two 2D materials is ambiguous, so the normalization is not as clear as for the other interfaces. Instead, formation energy for 2D|2D lateral interfaces is normally given with respect in eV/Å, with the per unit length being the line along which the two 2D materials bond. These formation energies (using interface length L instead of area S) result in $E_{\text{form,b}}$ and $E_{\text{form,s}}$ of 0.934 and −0.719 eV/Å, respectively.

B. Band alignment

The electronic properties are strongly influenced by the surface termination and, thus, the interface formed from these surfaces. Our principle focus here is on the difference between lateral and stacked alignment as these are the two extrema which these materials can form an interface at and thus present the most significant differences. By studying the local potential of the combined heterostructure, in addition to the individual constituents, we can identify the band offset between HfS_2 and HfO_2. The hole affinities of the isolated slabs are seen in Fig. 2. We compare the offsets predicted by Anderson's rule to those calculated and present this in Table I. As seen in Fig. 3, the band alignment is dependent on not only the terminations, but also the interactions of these two constituents.

Our results show that all four lateral interfaces exhibit type-I band alignment (straddled gap), in which the HfO_2 gap straddles the HfS_2 gap [see Figs. 3(a)–3(d)]. For each of these four heterostructures, we see quite strong disagreement with the expected band offset from those predicted by Anderson's rule. For interface A, we expect a band offset of 0.32 eV (type-I band alignment, with HfS_2 being responsible for both the valence- and conduction-band edges). However, we, instead find an offset of 1.9 eV, which is far greater than that expected from Anderson's rule. Interface B is expected to have a band offset of −0.07 eV (type II, with HfO_2 dominating the valence-band edge, and HfS_2 dominating the conduction-band edge); the heterostructure exhibits an offset of 1.64 eV. Interface C should exhibit an offset of 0.76 eV (type I, with HfS_2 dominating the valence and conduction edges); instead,

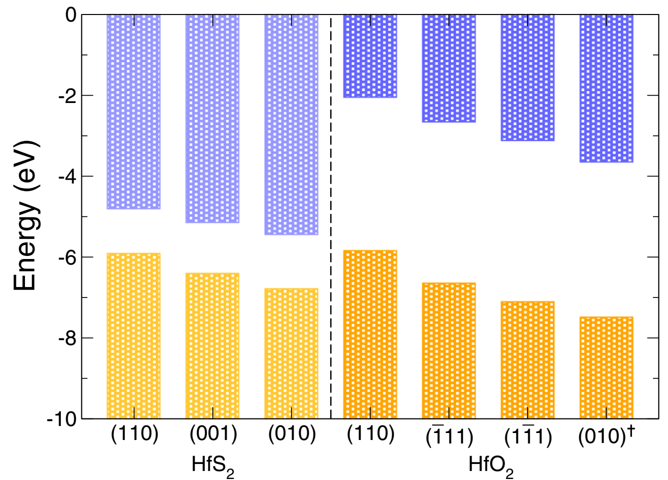

FIG. 2. Band positions (electron and hole affinities) of the individual strained constituent slabs as calculated from first principles using the PBE functional. The HfO_2 (010)† refers to a theoretical 2D-layered T-phase form of HfO_2, while the other HfO_2 slabs are modeled using the 3D monoclinic phase. Energy is given with respect to the vacuum energy.

the heterostructure exhibits an offset of 1.56 eV. For interface D, we expect a band offset of 0.7 eV. However, from Fig. 3(d), we see a band offset of 1.8 eV, over double that of the expected value.

For the two stacked interfaces, our results show E has type-II alignment and F has type-I alignment. Both of these heterostructures display relatively good agreement with the expected band offset as obtained from Anderson's rule. For interface E, we expect a band offset of −0.56 eV (type-II band alignment with HfO_2 dominating the valence-band edge, and HfS_2 dominating the conduction-band edge), which matches the offset seen in heterostructure. With interface F, we expect a 0.24 eV band offset (type-I band alignment with HfS_2 contributing the valence- and conduction-band edges); we find an offset of 0.26 eV, which is in close agreement.

The large shift in band offset from what is expected is likely caused by charge transfer across the interface. For the 2D/3D and 2D/2D lateral systems, we expect trans-interfacial chemical bonding. However, for the stacked system, we expect very few, or weak, trans-interfacial bonds (likely mediated by weak van der Waals interactions). The weaker the trans-interfacial bond, the less charge transfer we expect to see between the two constituent materials and, hence, the more similar the constituents are to their noninteracting slabs. As such, the stacked systems agree with Anderson's rule, but as soon as chemical bonds form, Anderson's rule is broken. The breakdown of this rule is what leads to the dramatic shifts in alignment seen in the lateral heterostructures. However, for all heterostructures, the expected band alignment type is maintained, with the exception of interface B and this could be due to the substantial atomic reconstruction.

To further investigate the breakdown of Anderson's rule for lateral systems, we compare the charge transfer for the lateral and stacked interfaces, as shown in Fig. 4. We see that, for the lateral interface, the transfer of charge is over one order of magnitude greater than that seen in the stacked system. This is

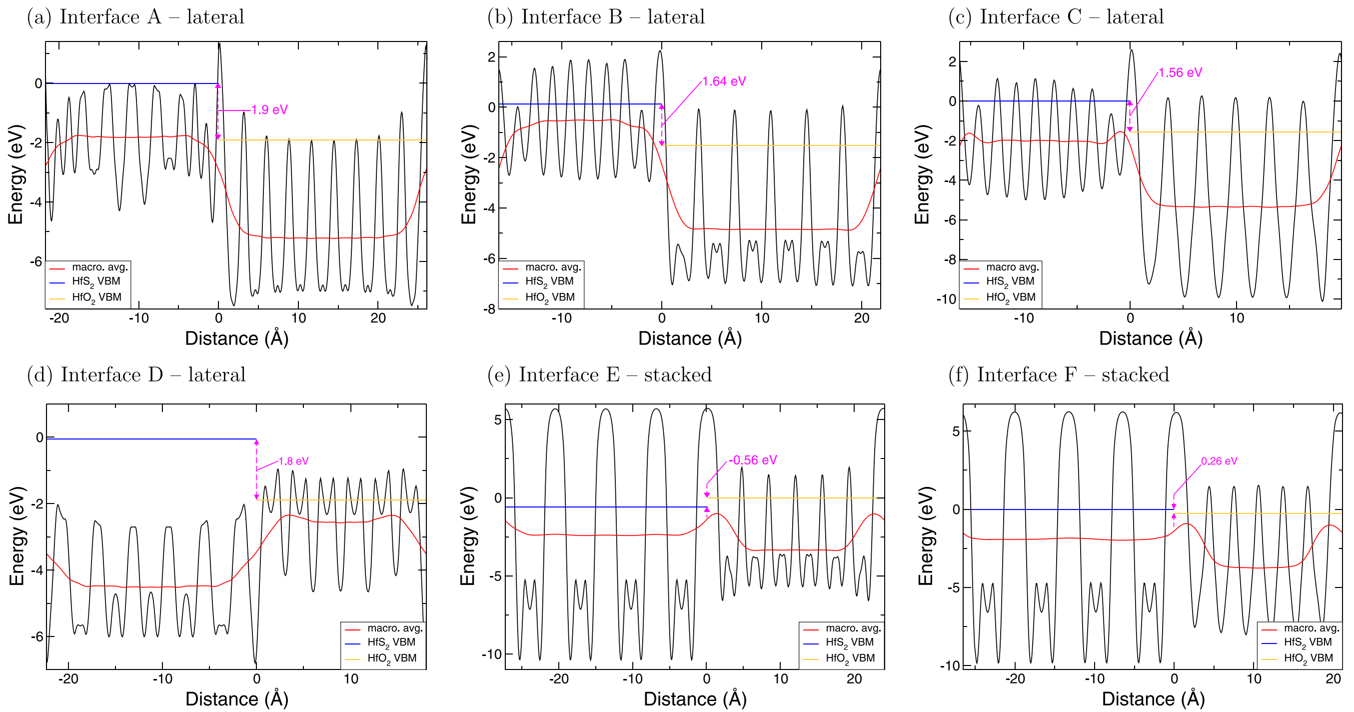

FIG. 3. Local potential plots for $HfS_2|HfO_2$ heterostructures, denoting the band offset. (a) $(010)/(1\bar{1}1)$, (b) (110)/(110), (c) $(110)/(\bar{1}11)$, (d) (010)/(010)–2D, (e) (001)/(110), and (f) $(001)/(\bar{1}11)$. For each subfigure, the energy scale is given with respect to its heterostructure's valence-band maximum. Distances are give with respect to the center of one of the interfaces in the cell, with the other interface found at the two presented extremes of the x axis (after which values, the structure repeats due to periodicity).

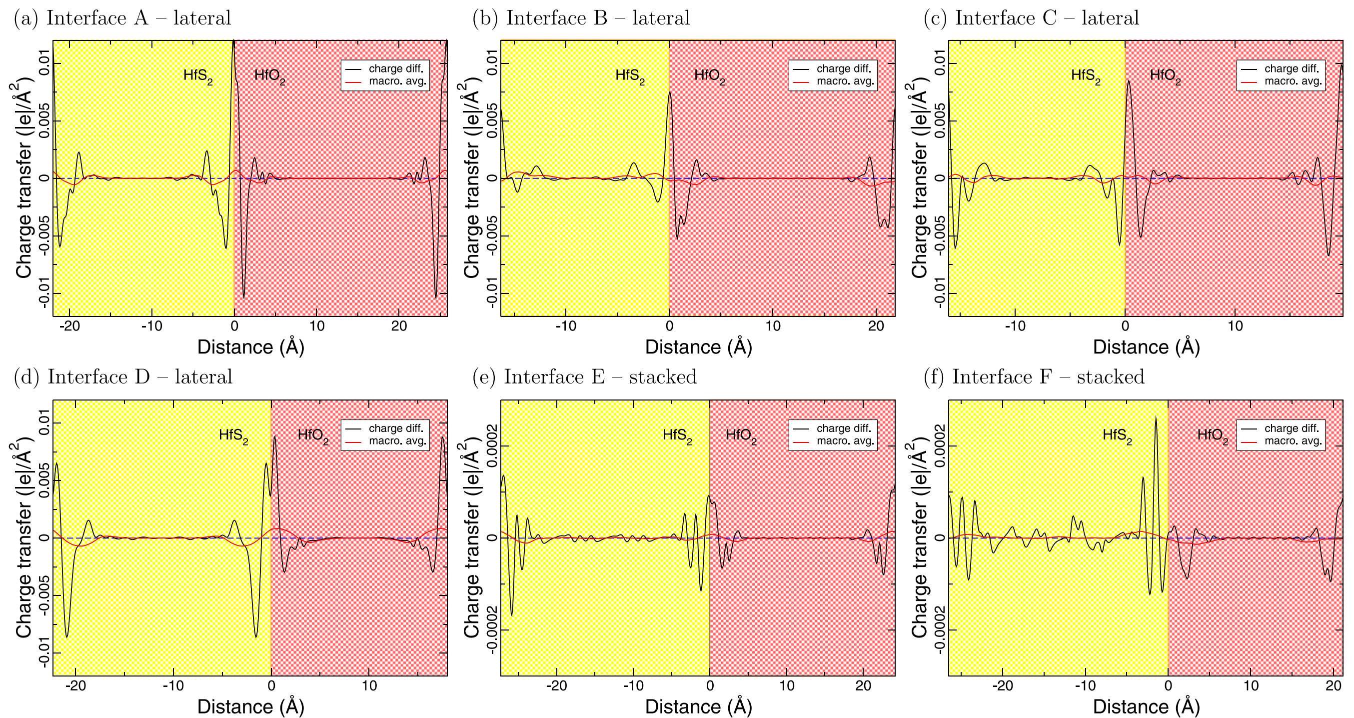

FIG. 4. Charge-transfer plots for the $HfS_2|HfO_2$ heterostructures. The (a) $(010)/(1\bar{1}1)$, (b) (110)/(110), (c) $(110)/(\bar{1}11)$, (d) (010)/(010)–2D, (e) (001)/(110), and (f) $(001)/(\bar{1}11)$ heterostructures. The blue dashed line denotes zero charge transfer, while the red line denotes the macroscopic average of the 1D planar-averaged charge transfer (black line). Positive values correspond to an increase in number of electrons in the heterostructure, while negative values correspond to a decrease in electrons. Distances are given with respect to the center of one of the interfaces in the cell, with the other interface found at the two presented extremes of the x axis (after which values, the structure repeats due to periodicity).

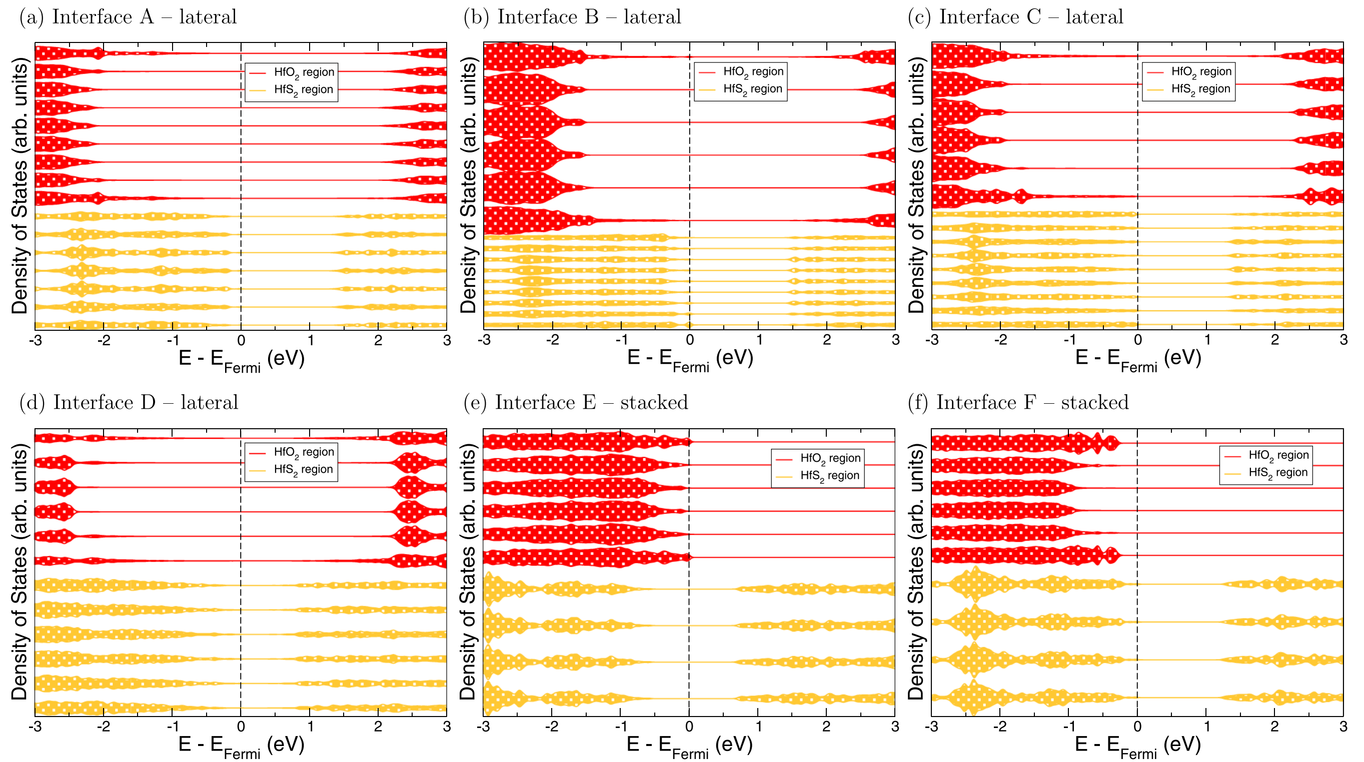

FIG. 5. Layer-projected densities of states for the $HfS_2|HfO_2$ heterostructures. The (a) (010)/(1$\bar{1}$1), (b) (110)/(110), (c) (110)/($\bar{1}$11), (d) (010)/(010)–2D, (e) (001)/(110), and (f) (001)/($\bar{1}$11) heterostructures. Due to the periodicity of the structure, the top layer of HfO_2 also borders the bottom layer of HfS_2 in each system, i.e., the second interface in the periodic cell.

likely due to stronger trans-interfacial bonding in the former system. This adds to the hypothesis that the change in band alignment from what is expected when considering just the isolated slabs is caused by greater amounts of charge transfer between the two materials, leading to significant electronic reconstruction.

In the lateral systems, we see that both the HfS_2 and HfO_2 transfer electrons to the interface, causing their surface atoms to lose electrons. For the two stacked systems, we see far fewer electrons transferred to the interface region. There is around a factor of 100 difference of charge transfer between lateral and stacked heterostructures. Conversely, for the stacked heterostructures, we see little change in the charge on the HfS_2, with its charge mostly redistributing along its Hf–S bonds. For the HfO_2, we see a net loss in electrons for its surface atoms. The interface in these heterostructures show slight net increase in the number of electrons.

We attribute the change in band alignment of lateral systems from Anderson's rule to the more significant transfer of charge. The stacked system exhibits charge transfer an order of magnitude smaller than the lateral system. In all systems, we see little change in the charge distribution in the HfO_2. For the stacked heterostructures, we see more significant charge redistribution in the HfS_2 regions.

To fully understand the effects of bonding on the $HfS_2|HfO_2$ heterostructures, we explore their electronic structures and potential electronic reconstructions caused by trans-interface bonding. With layer-projected densities of states, we can also identify how far the interface influence reaches. By comparing the heterostructures' densities of states to their corresponding slabs, we can identify perturbations from the isolated slabs and attribute these to interface effects or interactions. In Fig. 5 we see that the LDOSes also shows all systems are type-I alignment with the exception of D, which is type II. We also observe that most systems electronic structure results in either the high-energy valence and/or low-energy conduction states being dimensionally confined.

All four lateral interfaces, due to their type-I alignment, have HfS_2 states dominating near the valence- and conduction-band edges [see Figs. 5(a)–5(d)]. As HfO_2 has a very large band gap, it only contributes to states below -1.5 eV and above 2 eV (with respect to the valence-band maximum), whereas the HfS_2 band edges lie at 0 and $\approx$1.3 eV and are thus dominant. The density of states for these heterostructures are roughly symmetric about the band gap. We see only minor changes to the electronic states of HfS_2 far from the interfaces. At the interface, we see more significant change to the HfS_2 states, but similar reconstruction appears in the respective slab (see Fig. S5 [46]) indicating this is more a surface effect than attributable to interface bonding. Similarly, as one might expect, HfO_2 states appear unaffected by the interface far from it. However, states at the interface appear to reconstruct quite significantly, with a clear bleeding of HfS_2 states into the HfO_2 gap, which is not present in their respective slabs (see Fig. S6 [46]). For these lateral interfaces, with the exception of D (the 2D|2D system), we observe that the states attributed to HfS_2 are low in concentration and, as such, are drowned out by the HfO_2 states in the energy ranges where both are present. This is a result of the HfO_2 being a 3D material with a higher atomic density than 2D

HfS_2, correlating to a higher number of states per unit volume. For the lateral interfaces, we identify that the influence of the interface reaches two layers deep into the HfS_2 and one layer deep into the HfO_2.

For the two stacked interfaces, the HfO_2 valence states are closer to the valance-band maxima than in the lateral interfaces [see Figs. 5(e) and 5(f)]. For both, the unoccupied HfO_2 states are in excess of 3 eV above the Fermi energy. As such, it is likely that most of the conduction-electron properties will be dominated by the HfS_2 states. In both stacked interfaces, we see little change in the HfS_2 states, even at the interface. For interfaces E and F, the HfO_2 conduction states are present above 3.85 and 3.76 eV, respectively (with respect to the systems' valence-band maxima, see Fig. S11 [46]). We see more substantial changes in the HfO_2 valence states near the interface, however, when compared with their respective slabs, which is likely attributed to dangling bonds. Interface E is unique in that this type-II alignment has resulted in a $\approx$0.5 eV offset between the HfS_2 and HfO_2 states in the valence band, with the HfS_2 states falling below the HfO_2, which is unlike any of the other cases. For interface F, we find that the HfO_2 valence states only fall around 0.26 eV below the HfS_2 valence states, resulting in its type-I alignment. When comparing the stacked heterostructure to the constituent slabs, we see far less change to the densities of states than what was seen for the lateral system. This is likely caused by the greater separation between the two slabs and the change from chemical bonding (in the lateral) to van der Waals bonding (in the stacked), resulting in less electronic reconstruction and fewer interfacial states arising. For the stacked interfaces, there is minimal electronic reconstruction and, as such, the interface has no measurable influence on either material.

Figure 5(a) shows the layer-projected density of states of interface A. While HfS_2 contributes to both the valence- and conduction-band edges, HfO_2 only starts to contribute to states below -1 eV and above 2 eV (with respect to the valence-band maximum). The interactions between HfS_2 and HfO_2 across the interface in interface A causes changes to the constituent electronic densities of states. This heterostructure sees a suppression of surface states for HfS_2. This is shown by comparing Fig. S5(a) with Fig. 5(a), where the isolated slab shows an increase in the number of states at the valence-band edge, contrasting a suppression of states in the heterostructure, particularly in the range of -1 to 0 eV (with respect to the valence-band maximum). When comparing Fig. S6(a) to Fig. 5(a), it can be seen that the surface states of HfO_2 see a significant change; there appears to be considerable introduction of new states above the valence-band edge of the HfO_2, likely caused by either bleeding in of HfS_2 states or introduction of new interfacial states due to trans-interfacial bonds.

By comparing interfaces B and E, we can explore how the change from type-I to type-II band alignment is influenced by the orientation of the HfS_2 (basal parallel or perpendicular) compared with the HfO_2. The LDOS, seen in Fig. 5(b), shows that the HfO_2 states straddle the HfS_2 states for interface B. Conversely for interface E [see Fig. 5(e)], we find that HfO_2 contributes the valence edge states, and the HfS_2 contribute the conduction edge states. The electronic properties of the central regions of the HfS_2 and HfO_2 in both heterostructures are well behaved, showing little change from those present in the isolated slabs [see Figs. S5(c), S5(d), and S6(b)] or their corresponding bulks (see Fig. S4). At the interface, reconstruction of the HfO_2 states are present in both systems, with both interfaces exhibiting slight smoothing of densities of states and an increase in state concentration closer to the valence-band maxima. In the stacked heterostructure (E), we see almost no reconstruction of HfS_2 states at the interface (with these minor changes visible in the isolated slab), whereas the lateral heterostructure (B) exhibits a smoothing of states, along with an increase in state concentration between -1 and 0 eV. In interface E, the minor HfO_2 electronic reconstruction is consistent with that seen in the isolated slab, suggesting little interaction between the HfS_2 and HfO_2 slabs. In interface B, there is more substantial electronic reconstruction distinct from that seen in the isolated slabs, and we see a raising of the occupied states into the HfO_2 gap, likely caused by chemical bonds forming across the interface.

Interface B shows a slight asymmetry between its two interfaces. In the lower interface, the HfS_2 sees new states present at the top of the VBM that are not present in the central interface [see Fig. S7(a)]. However, this electronic structure of HfS_2 at the lower interface is similar to that seen in the isolated slab [see Fig. S5(c)], suggesting that the central interface involves a larger amount of electronic reconstruction. This minor asymmetry present in the valence states of interface B results in a slight electric field across this system of around 0.02 eV/Å.

Again, to compare two similar HfO_2 surfaces in lateral and stacked interfaces, we discuss the electronic changes associated with interfaces C and F [see Figs. 5(c) and 5(f)]. While both of these heterostructures display type-I band alignment, in F the surface valence states of HfO_2 are almost perfectly aligned with those of HfS_2 (with F just barely being type-I aligned). We see a lot of similarities between the comparison of this pair of heterostructures (C and F) and the previous pair (B and E), including the asymmetric electronic reconstruction of the lateral interfaces, the lack of electronic reconstruction of the stacked systems, and the suppression of HfS_2 surface states in the lateral system attributed to bond compensation. Here, surface states of the HfO_2 are suppressed in one of the interfaces (the lower), while both the interfaces exhibit HfS_2 surface state suppression [see Figs. S5(c), S5(d), and S6(c)]. As with the previous pairing, the valence states in the lateral heterostructure exhibit more reconstruction than the conduction states. In the stacked system (F), the HfS_2 dominates the lower conduction region, while the valence region is contributed to jointly by HfS_2 and HfO_2.

Interface D is a unique case as it consists of a 2D|2D interface. The electronic configuration of interface D is similar to that of A, both exhibit type-I band alignment, in which the HfO_2 gap straddles the HfS_2 gap (with HfS_2 being the dominant contributor to states in an energy window of -2 to 2 eV about the valence-band maxima). Furthermore, both exhibit comparable alignment (1.90 and 1.80 eV for A and D, respectively), and similar electronic reconstruction for the HfS_2 and HfO_2 near-interface states, with a reduction in HfS_2 valence and conduction state concentration.

However, for the 2D/2D system (D), we note several unusual characteristics, most notably the band gap is smaller

than in the 2D|3D cases (≈0.43 vs ≈1.3 eV). To identify the origin of this significant change in gap size, we have considered the effect of including the van der Waals correction, tilting, and shear strains. For interface D, we repeated the relaxation and electronic calculations with and without the DFT-D3 vdW correction [64] to assess whether this gap reduction was a result of the choice of functional. However, the same gap of 0.43 eV is obtained using either approach (see Fig. S10 [46]). In Fig. S9 [46], we present a 2D|2D interface that has a reduced anisotropic strain for the HfS_2, coinciding with a smaller smoothing of HfS_2 states and a smaller reduction of band gap. As such, it is likely that the decreased gap observed in the HfS_2 region is due to the anisotropic strain on the HfS_2 layers. The tilting also results in a reduced basal spacing from a vdW corrected value of 5.87 to 5.70 Å, which would strengthen interlayer interactions. We see that this reduced gap does not relate to interface states, as all of the HfS_2 layers exhibit the same band gap of 0.43 eV [see Fig. 5(d)]. Thus, it is most likely that this reduced gap is a result of anisotropic strain on the HfS_2 layers.

We next identify how the character of the states of interface D change due to the anisotropic shear strain. Our results also show that the states relating to the reduced HfS_2 gap are low in density and appear just below the valence-band edge. The HfS_2 states exhibit substantial reconstruction, losing most features present in the equivalent slab and the density of states becoming smoothed out [see Fig. S5(a)]—these changes to the character remain for the strained isolated slab, so are not caused by interface interactions [see Fig. S5(b)]. The HfO_2 states in the middle of the region appear consistent with the density of states of the isolated slab [see Fig. S6], indicating these are bulk 2D like. However, the surface states are drastically different, with large surface states at the valence band edge being strongly suppressed in the heterostructure.

Our results show that, while lateral junctions are type I, stacked junctions are either type I or type II with minimal difference in the valance band offset between the two regions. These two types of junctions have interesting consequences for charge transport across the interfaces, particularly for optical excitations such as excitons. For absorptions in the very near interface region, one can expect lower frequencies to be absorbed than either of the two constituents band gaps, but as this region by volume is very small, this contribution should be minor. Conversely, the creation of excitons will result in most excitons being trapped in the HfS_2 regions, but being split by the layer-upon-layer (stacked) boundary. It is perhaps a surprising result that the chemically bonded interfaces will result in excitons being confined, but traveling perpendicular from the HfS_2 layer into HfO_2 (or vice versa) will result in charge separation. This suggests that, in real samples consisting of multiple interfaces, exciton splitting could occur simply due to the presence of just a stacked interface, without the need for dopants. This, in turns, suggests that doping could be used to enhance or further adjust these effects. Furthermore, the range in barrier heights for the in plane interfaces is 2.46 eV, and this variety of barrier heights is undoubtedly larger in real systems, but it remains to be seen if it could exceed the range provided here.

IV. CONCLUSION

Overall, we have modeled a variety of HfS_2|HfO_2 interfaces, exploring how 2D|3D interfaces behave. Our results have shown that there exists almost no electronic reconstruction when layers of HfS_2 are placed on a HfO_2 substrate. Conversely, when the connection between HfO_2 and HfS_2 is made, there is a more significant interface reconstruction present in the lateral system than the stacked. In the latter case all examples considered yielded a type-II alignment, whereas in the case that layers were parallel to the HfO_2 substrate (stacked) we found that the alignment was either type I or type II with a very small difference between the valance bands of the two constituents.

Here, we have explored interfaces between 2D HfS_2 and 3D HfO_2, and shown how the band alignment is dependent on crystal surface termination. While stacked HfS_2|HfO_2 heterostructures show relative agreement with Anderson's rule (as is the case for many stacked 2D TMDC heterostructures), lateral HfS_2|HfO_2 heterostructures do not. We explore the electronic properties of various HfS_2|HfO_2 interfaces and attribute the breaking of Anderson's rule to a significant increase in charge transfer across the interface. We have tried to remove all variables of the heterostructures to focus solely on the crystal orientation at the interface. By mitigating other potential factors, we show that the only change between the lateral and stacked interfaces is the charge transfer. These results provide a fundamental understanding of the electronic properties of HfS_2 HfO_2 interfaces and show how the surface termination and orientation of 2D|3D interfaces can have quite dramatic effects on the band alignment. These results shown that fabrication will be key and, in turn, allow for tunable band alignments and better control of electronic and optical devices for these 2D|3D interfaces.

The data that support the findings of this study are openly available from the University of Exeter's Institutional repository [80].

ACKNOWLEDGMENTS

The authors thank the Leverhulme for funding this research via Grant No. RPG-2021-086. Via our membership of the UK's HEC Materials Chemistry Consortium, which is funded by EPSRC (EP/R029431), this work used the ARCHER2 UK National Supercomputing Service [81]. The authors would also like to acknowledge the use of the University of Exeter High-Performance Computing (HPC) facility in carrying out this work. Data retrieved from the Materials Project for HfS_2 (mp-985829) and HfO_2 (mp-352) from database version v2022.10.28.

[1] S. Lai, S. Byeon, S. K. Jang, J. Lee, B. H. Lee, J.-H. Park, Y.-H. Kim, and S. Lee, HfO_2/HfS_2 hybrid heterostructure fabricated *via* controllable chemical conversion of two-dimensional HfS_2, Nanoscale **10**, 18758 (2018).

[2] A. De Sanctis, I. Amit, S. P. Hepplestone, M. F. Craciun, and S. Russo, Strain-engineered inverse charge-funnelling in layered semiconductors, Nat. Commun. **9**, 1652 (2018).

[3] Y. Y. Wang, S. M. Huang, K. Yu, J. Jiang, Y. Liang, B. Zhong, H. Zhang, G. F. Kan, S. F. Quan, and J. Yu, Atomically flat HfO_2 layer fabricated by mild oxidation HfS_2 with controlled number of layers, J. Appl. Phys. **127**, 214303 (2020).

[4] O. Song, D. Rhee, J. Kim, Y. Jeon, V. Mazánek, A. Söll, Y. A. Kwon, J. H. Cho, Y.-H. Kim, Z. Sofer, and J. Kang, All inkjet-printed electronics based on electrochemically exfoliated two-dimensional metal, semiconductor, and dielectric, npj 2D Mater. Appl. **6**, 64 (2022).

[5] X. Zhao and D. Vanderbilt, First-principles study of structural, vibrational, and lattice dielectric properties of hafnium oxide, Phys. Rev. B **65**, 233106 (2002).

[6] P. W. Peacock and J. Robertson, Band offsets and Schottky barrier heights of high dielectric constant oxides, J. Appl. Phys. **92**, 4712 (2002).

[7] J. Robertson, High dielectric constant oxides, Eur. Phys. J.: Appl. Phys. **28**, 265 (2004).

[8] J. Robertson, High dielectric constant gate oxides for metal oxide Si transistors, Rep. Prog. Phys. **69**, 327 (2006).

[9] H. Zhu, C. Tang, L. R. C. Fonseca, and R. Ramprasad, Recent progress in ab initio simulations of hafnia-based gate stacks, J. Mater. Sci. **47**, 7399 (2012).

[10] J. Robertson and R. M. Wallace, High-K materials and metal gates for CMOS applications, Mater. Sci. Eng., R **88**, 1 (2015).

[11] H. Wang, L. Yu, and T. Palacios, Large-scale 2D electronics based on single-layer MoS_2 grown by chemical vapor deposition, in *2012 International Electron Devices Meeting, San Francisco, San Francisco, CA* (IEEE, Piscataway, NJ, 2012), pp. 4.6.1–4.6.4.

[12] Z. Geng, W. Kinberger, R. Granzner, J. Pezoldt, and F. Schwierz, 2D Electronics—Opportunities and Limitations, in *2016 46th European Solid-State Device Research Conference (ESSDERC), Lausanne, Switzerland* (IEEE, Piscataway, NJ, 2016), pp. 230–235.

[13] Y. Y. Illarionov, T. Knobloch, M. Jech, M. Lanza, D. Akinwande, M. I. Vexler, T. Mueller, M. C. Lemme, G. Fiori, F. Schwierz, and T. Grasser, Insulators for 2D nanoelectronics: The gap to bridge, Nat. Commun. **11**, 3385 (2020).

[14] W. Gee Kim, M. Gyu Sung, S. Joo Kim, J. Hee Yoo, T. One Youn, J. Won Oh, J. Nam Kim, B. Gu Gyun, T. Wan Kim, C. Ho Kim, J. Young Byun, W. Kim, M. Sig Joo, J. Sung Roh, and S. Ki Park, Dependence of the switching characteristics of resistance random access memory on the type of transition metal oxide; TiO_2, ZrO_2, and HfO_2, J. Electrochem. Soc. **158**, H417 (2011).

[15] V. Mladenov, A New Simplified Model for HfO_2-Based Memristor, in *2019 8th International Conference on Modern Circuits and Systems Technologies (MOCAST), Thessaloniki, Greece* (IEEE, Piscataway, NJ, 2019), pp. 1–4.

[16] A. Saleem, D. Kumar, A. Singh, S. Rajasekaran, and T.-Y. Tseng, Oxygen vacancy transition in HfO_x-based flexible, robust, and synaptic bi-layer memristor for neuromorphic and wearable applications, Adv. Mater. Technol. (Weinheim, Ger.) **7**, 2101208 (2022).

[17] D. Wang, X. Zhang, H. Liu, J. Meng, J. Xia, Z. Yin, Y. Wang, J. You, and X.-M. Meng, Epitaxial growth of HfS_2 on sapphire by chemical vapor deposition and application for photodetectors, 2D Mater. **4**, 031012 (2017).

[18] C. Yan, L. Gan, X. Zhou, J. Guo, W. Huang, J. Huang, B. Jin, J. Xiong, T. Zhai, and Y. Li, Space-confined chemical vapor deposition synthesis of ultrathin HfS_2 flakes for optoelectronic application, Adv. Funct. Mater. **27**, 1702918 (2017).

[19] K. Xu, Y. Huang, B. Chen, Y. Xia, W. Lei, Z. Wang, Q. Wang, F. Wang, L. Yin, and J. He, Toward high-performance top-gate ultrathin HfO_2 field-effect transistors by interface engineering, Small **12**, 3106 (2016).

[20] T. Kanazawa, T. Amemiya, V. Upadhyaya, A. Ishikawa, K. Tsuruta, T. Tanaka, and Y. Miyamoto, Performance improvement of HfS_2 transistors by atomic layer deposition of HfO_2, IEEE Trans. Nanotechnol. **16**, 582 (2017).

[21] Y. M. Jahn and A. Ya'akobovitz, Outstanding stretchability and thickness-dependent mechanical properties of 2d HfS_2, $HfSe_2$, and hafnium oxide, Nanoscale **13**, 18458 (2021).

[22] M. Leem, H. Lee, T. Park, W. Ahn, H. Kim, E. Lee, and H. Kim, Intriguing morphological evolution during chemical vapor deposition of HfS_2 using $HfCl_4$ and S on sapphire substrate, Appl. Surf. Sci. **509**, 144701 (2020).

[23] H. Wang, F. Liu, W. Fu, Z. Fang, W. Zhou, and Z. Liu, Two-dimensional heterostructures: Fabrication, characterization, and application, Nanoscale **6**, 12250 (2014).

[24] K. S. Novoselov, A. Mishchenko, A. Carvalho, and A. H. Castro Neto, 2D materials and van der Waals heterostructures, Science **353**, aac9439 (2016).

[25] A. Chaves, J. G. Azadani, H. Alsalman, D. R. da Costa, R. Frisenda, A. J. Chaves, S. H. Song, Y. D. Kim, D. He, J. Zhou, A. Castellanos-Gomez, F. M. Peeters, Z. Liu, C. L. Hinkle, S.-H. Oh, P. D. Ye, S. J. Koester, Y. H. Lee, P. Avouris, X. Wang *et al.*, Bandgap engineering of two-dimensional semiconductor materials, npj 2D Mater. Appl. **4**, 29 (2020).

[26] A. H. Proppe, A. Johnston, S. Teale, A. Mahata, R. Quintero-Bermudez, E. H. Jung, L. Grater, T. Cui, T. Filleter, C.-Y. Kim, S. O. Kelley, F. De Angelis, and E. H. Sargent, Multication perovskite 2D/3D interfaces form via progressive dimensional reduction, Nat. Commun. **12**, 3472 (2021).

[27] K. Reidy, G. Varnavides, J. D. Thomsen, A. Kumar, T. Pham, A. M. Blackburn, P. Anikeeva, P. Narang, J. M. LeBeau, and F. M. Ross, Direct imaging and electronic structure modulation of moiré superlattices at the 2D/3D interface, Nat. Commun. **12**, 1290 (2021).

[28] P. V. Pham, S. C. Bodepudi, K. Shehzad, Y. Liu, Y. Xu, B. Yu, and X. Duan, 2D heterostructures for ubiquitous electronics and optoelectronics: Principles, iopportunities, and challenges, Chem. Rev. (Washington, DC, US) **122**, 6514 (2022).

[29] L.-X. Zhou, Y.-T. Ren, Y.-T. Chen, X.-H. Lv, C.-D. Jin, H. Zhang, P.-L. Gong, R.-Q. Lian, R.-N. Wang, J.-L. Wang, and X.-Q. Shi, Quasi-bonding-induced gap states in metal/two-dimensional semiconductor junctions: route for Schottky barrier height reduction, Phys. Rev. B **105**, 224105 (2022).

[30] H. Zhu, Z. Hong, C. Zhou, Q. Wu, T. Zheng, L. Yang, S. Lan, and W. Yang, Energy band alignment of 2D/3D MoS_2/4H-SiC heterostructure modulated by multiple interfacial interactions, Front. Phys. **18**, 13301 (2023).

[31] B. Zheng, Y. Chen, Z. Wang, F. Qi, Z. Huang, X. Hao, P. Li, W. Zhang, and Y. Li, Vertically oriented few-layered HfS_2 nanosheets: Growth mechanism and optical properties, 2D Mater. **3**, 035024 (2016).

[32] B. Zheng, Z. Wang, F. Qi, X. Wang, B. Yu, W. Zhang, and Y. Chen, CVD growth of large-area and high-quality HfS_2 nanoforest on diverse substrates, Appl. Surf. Sci. **435**, 563 (2018).

[33] R. L. Anderson, Germanium-gallium arsenide heterojunctions [Letter to the editor], IBM J. Res. Dev. **4**, 283 (1960).

[34] N. F. Mott, Note on the contact between a metal and an insulator or semi-conductor, Math. Proc. Cambridge Philos. Soc. **34**, 568 (1938).

[35] W. Schottky, Vereinfachte und erweiterte Theorie der Randschicht-gleichrichter, Eur. Phys. J. A **118**, 539 (1942).

[36] J. Bardeen, Surface states and rectification at a metal semi-conductor contact, Phys. Rev. **71**, 717 (1947).

[37] S. G. Louie and M. L. Cohen, Electronic structure of a metal-semiconductor interface, Phys. Rev. B **13**, 2461 (1976).

[38] A. Baldereschi, S. Baroni, and R. Resta, Band Offsets in Lattice-Matched Heterojunctions: A Model and First-Principles Calculations for GaAs/AlAs, Phys. Rev. Lett. **61**, 734 (1988).

[39] W. R. L. Lambrecht and B. Segall, Theory of Semiconductor Heterojunction Valence-Band Offsets: From Supercell Band-Structure Calculations toward a Simple Model, Phys. Rev. Lett. **61**, 1764 (1988).

[40] R. Resta, S. Barnoi, and A. Baldereschi, Theory of band offsets at semiconductor heterojunctions: An *ab-initio* linear response approach, Superlattices Microstruct. **6**, 7 (1989).

[41] Y. Hinuma, A. Grüneis, G. Kresse, and F. Oba, Band alignment of semiconductors from density-functional theory and many-body perturbation theory, Phys. Rev. B **90**, 155405 (2014).

[42] L. Weston, H. Tailor, K. Krishnaswamy, L. Bjaalie, and C. Van de Walle, Accurate and efficient band-offset calculations from density functional theory, Comput. Mater. Sci. **151**, 174 (2018).

[43] W. Mönch, On the band-structure lineup at Schottky contacts and semiconductor heterostructures, Mater. Sci. Semicond. Process. **28**, 2 (2014).

[44] K. Xu, Y. Xu, H. Zhang, B. Peng, H. Shao, G. Ni, J. Li, M. Yao, H. Lu, H. Zhu, and C. M. Soukoulis, The role of Anderson's rule in determining electronic, optical and transport properties of transition metal dichalcogenide heterostructures, Phys. Chem. Chem. Phys. **20**, 30351 (2018).

[45] F. H. Davies, C. J. Price, N. T. Taylor, S. G. Davies, and S. P. Hepplestone, Band alignment of transition metal dichalcogenide heterostructures, Phys. Rev. B **103**, 045417 (2021).

[46] See Supplemental Material at http://link.aps.org/supplemental/10.1103/PhysRevB.107.205302 for further details and discussions (see also Refs. [65–79]). The topics covered include: nomenclature, lattice matching, energetics and electronic properties of the bulk crystals and unstrained slabs, additional heterostructures, the effects of including a van der Waals correction, and the effect of different chemical environments on interface formation energy.

[47] G. Kresse and J. Furthmüller, Efficient iterative schemes for *ab initio* total-energy calculations using a plane-wave basis set, Phys. Rev. B **54**, 11169 (1996).

[48] G. Kresse and J. Furthmüller, Efficiency of ab-initio total energy calculations for metals and semiconductors using a plane-wave basis set, Comput. Mater. Sci. **6**, 15 (1996).

[49] J. P. Perdew, K. Burke, and M. Ernzerhof, Generalized Gradient Approximation Made Simple, Phys. Rev. Lett. **77**, 3865 (1996).

[50] The Materials Project, Materials Data on HfS_2 by Materials Project (2020), https://doi.org/10.17188/1316755.

[51] The Materials Project, Materials Data on HfO_2 by Materials Project (2020), https://doi.org/10.17188/1206948.

[52] D. L. Greenaway and R. Nitsche, Preparation and optical properties of GroupIV $-$ VI_2 chalcogenides having the CdI_2 structure, J. Phys. Chem. Solids **26**, 1445 (1965).

[53] J. Adam and M. D. Rogers, The crystal structure of ZrO_2 and HfO_2, Acta Crystallogr. **12**, 951 (1959).

[54] M. Balog, M. Schieber, M. Michman, and S. Patai, Chemical vapor deposition and characterization of HfO_2 films from organo-hafnium compounds, Thin Solid Films **41**, 247 (1977).

[55] N. T. Taylor, F. H. Davies, I. E. M. Rudkin, C. J. Price, T. H. Chan, and S. P. Hepplestone, Artemis: *Ab Initio* restructuring tool enabling the modelling of interface structures, Comput. Phys. Commun. **257**, 107515 (2020).

[56] K. T. Delaney, N. A. Spaldin, and C. G. Van de Walle, Theoretical study of Schottky-barrier formation at epitaxial rare-earth-metal/semiconductor interfaces, Phys. Rev. B **81**, 165312 (2010).

[57] M. S. Hybertsen, Role of interface strain in a lattice-matched heterostructure, Phys. Rev. Lett. **64**, 555 (1990).

[58] K. S. Vasu, E. Prestat, J. Abraham, J. Dix, R. J. Kashtiban, J. Beheshtian, J. Sloan, P. Carbone, M. Neek-Amal, S. J. Haigh, A. K. Geim, and R. R. Nair, Van der Waals pressure and its effect on trapped interlayer molecules, Nat. Commun. **7**, 12168 (2016).

[59] S. Pramchu, A. P. Jaroenjittichai, and Y. Laosiritaworn, DFT calculations of strain and interface effects on electronic structures and magnetic properties of $L1_2$-FePt/Ag heterojunction of GMR applications, AIP Adv. **8**, 035310 (2018).

[60] Y. Zhang, W. Si, Y. Jia, P. Yu, R. Yu, and J. Zhu, Controlling strain relaxation by interface design in highly lattice-mismatched heterostructure, Nano Lett. **21**, 6867 (2021).

[61] K. Xiong, W. Wang, H. N. Alshareef, R. P. Gupta, J. B. White, B. E. Gnade, and K. Cho, Electronic structures and stability of Ni/Bi_2Te_2 and Co/Bi_2Te_3 interfaces, J. Phys. D: Appl. Phys. **43**, 115303 (2010).

[62] T. Björkman, A. Gulans, A. V. Krasheninnikov, and R. M. Nieminen, Are we van der Waals ready?, J. Phys.: Condens. Matter **24**, 424218 (2012).

[63] T. Björkman, A. Gulans, A. V. Krasheninnikov, and R. M. Nieminen, Van der Waals Bonding in Layered Compounds from Advanced Density-Functional First-Principles Calculations, Phys. Rev. Lett. **108**, 235502 (2012).

[64] S. Grimme, J. Antony, S. Ehrlich, and H. Krieg, A consistent and accurate *ab initio* parametrization of density functional dispersion correction (DFT-D) for the 94 elements H-Pu, J. Chem. Phys. **132**, 154104 (2010).

[65] B. R. Tuttle, *Ab initio* valence band offsets between Si(100) and SiO_2 from microscopic models, Phys. Rev. B **67**, 155324 (2003).

[66] M. Watarai, J. Nakamura, and A. Natori, Band discontinuity at ultrathin SiO_2/Si(001) interfaces, Phys. Rev. B **69**, 035312 (2004).

[67] F. Giustino and A. Pasquarello, Electronic and dielectric properties of a suboxide interlayer at the silicon–oxide interface in MOS devices, Surf. Sci. **586**, 183 (2005).

[68] S. P. Hepplestone and P. V. Sushko, Effect of metal intermixing on the Schottky barriers of Mo(100)/GaAs(100) interfaces, J. Appl. Phys. **116**, 193703 (2014).

[69] M. N. Gjerding, L. S. R. Cavalcante, A. Chaves, and K. S. Thygesen, Efficient *ab initio* modeling of dielectric screening in 2D van der Waals materials: Including phonons, substrates, and doping, J. Phys. Chem. C **124**, 11609 (2020).

[70] A. Ohtake, Surface reconstructions on GaAs(001), Surf. Sci. Rep. **63**, 295 (2008).

[71] G.-X. Qian, R. M. Martin, and D. J. Chadi, First-principles study of the atomic reconstructions and energies of Aa- and As-stabilized GaAs(100) surfaces, Phys. Rev. B **38**, 7649 (1988).

[72] E. Heifets, J. Ho, and B. Merinov, Density functional simulation of the $BaZrO_3$ (011) surface structure, Phys. Rev. B **75**, 155431 (2007).

[73] E. A. D. Baker, J. Pitfield, C. J. Price, and S. P. Hepplestone, Computational analysis of the enhancement of photoelectrolysis using transition metal dichalcogenide heterostructures, J. Phys.: Condens. Matter **34**, 375001 (2022).

[74] I. Galanakis, G. Bihlmayer, V. Bellini, N. Papanikolaou, R. Zeller, S. Blügel, and P. H. Dederichs, Broken-bond rule for the surface energies of noble metals, Europhys. Lett. **58**, 751 (2002).

[75] Y. Y. Sun, H. Xu, Y. P. Feng, A. C. H. Huan, and A. T. S. Wee, Rule for Structures of Open Metal Surfaces, Phys. Rev. Lett. **93**, 136102 (2004).

[76] F. Ma and K.-W. Xu, Using dangling bond density to characterize the surface energy of nanomaterials, Surf. Interface Anal. **39**, 611 (2007).

[77] Z.-y. Gao, W. Sun, and Y. hua Hu, Mineral cleavage nature and surface energy: Anisotropic surface broken bonds consideration, Trans. Nonferrous Met. Soc. China **24**, 2930 (2014).

[78] A. Acosta, J. M. P. Martirez, N. Lim, J. P. Chang, and E. A. Carter, Relationship between ferroelectric polarization and stoichiometry of HfO_2 surfaces, Phys. Rev. Mater. **5**, 124417 (2021).

[79] K. Reuter and M. Scheffler, Composition, structure, and stability of RuO_2(110) as a function of oxygen pressure, Phys. Rev. B **65**, 035406 (2001).

[80] N. T. Taylor and S. P. Hepplestone, Effect of charge transfer on band alignment in 2D|3D heterostructures: A study of HfS_2|HfO_2 interfaces (dataset) (University of Exeter, 2023), https://doi.org/10.24378/exe.4644.

[81] https://www.archer2.ac.uk/.